

Ga droplet surface dynamics during Langmuir evaporation of GaAs

W.-X. Tang
C.-X. Zheng
Z.-Y. Zhou
D. E. Jesson
J. Tersoff

We describe the design and application of a low-energy electron microscope (LEEM) dedicated to the study of III–V materials. Recent studies of Langmuir (free) evaporation of GaAs(001) have been reviewed. Running Ga droplets are observed, and the motion is predicted and shown to slow and stop near a characteristic temperature. Striking bursts of “daughter” droplet nucleation accompany the coalescence of large “parent” droplets. These observations imply that evaporation and surface morphology are intimately connected, suggesting a new approach for the self-assembly and positioning of nanostructures on patterned surfaces.

Introduction

GaAs-based devices play a central role in radiofrequency communications technology and optoelectronics. Applications range from mobile phones and wireless networks to laser pointers and DVD players. GaAs high-electron-mobility transistors and III–V-based laser diodes can be viewed as the major components underlying modern communications and optoelectronics. Such structures are composed of thin layers of III–V semiconductor materials, which are grown by molecular beam epitaxy (MBE) with atomic-layer precision. Given the technological importance of III–V MBE growth, real-space imaging of surface growth dynamics is highly desirable. However, this has remained elusive largely because any imaging method must be compatible with the incident As flux, which is a characteristic of III–V MBE.

In parallel with advancing current technologies, longer term objectives in III–V research are to move beyond the constraints of conventional lithography and fabricate new quantum structures using variants of MBE. Quantum dots, double dots, rings, double rings, molecules, and rods have now been assembled [1–4] with potential applications including novel lasers, electron-spin memory, and quantum computing. However, a significant limitation in the realization of new quantum structures is our inability to observe how they form in real time and hence understand

how to tailor their characteristics. Just like interfaces grown by MBE, quantum structures are usually created under the As flux at elevated temperatures, and thus, imaging how they form under real growth conditions is highly desirable.

To facilitate imaging of a technologically important interface and quantum structure formation under the As flux, we have developed a surface electron microscope integrated with a III–V MBE system. In this paper, we describe the basic design of this III–V low-energy electron microscope (LEEM). Applications of III–V LEEM to the study of Langmuir (free) evaporation of GaAs into a vacuum are then reviewed, revealing the unexpected and striking motion of Ga droplets [5] and how decomposition is controlled by surface morphology during evaporation [6].

III–V LEEM system

The basic instrument consists of an Elmitec LEEM III configuration, which incorporates a Schottky field-emission electron source for enhanced brightness and beam coherence compared with the conventional LaB₆ gun. Incorporation of III–V MBE required significant modifications, including installation of multiple deposition sources, dedicated equipment for surface cleaning, and an internal cooling shroud to limit the buildup of As background pressure [7].

Figure 1(a) contains an overview of our instrument. A cross section of the basic LEEM system and the specimen region are shown in **Figures 1(b)** and **1(c)**, respectively.

The system is equipped with Ga and In effusion cells with integrated cooling shrouds and shutters and a metal valve

Digital Object Identifier: 10.1147/JRD.2011.2158762

© Copyright 2011 by International Business Machines Corporation. Copying in printed form for private use is permitted without payment of royalty provided that (1) each reproduction is done without alteration and (2) the Journal reference and IBM copyright notice are included on the first page. The title and abstract, but no other portions, of this paper may be copied by any means or distributed royalty free without further permission by computer-based and other information-service systems. Permission to republish any other portion of this paper must be obtained from the Editor.

0018-8646/11/\$5.00 © 2011 IBM

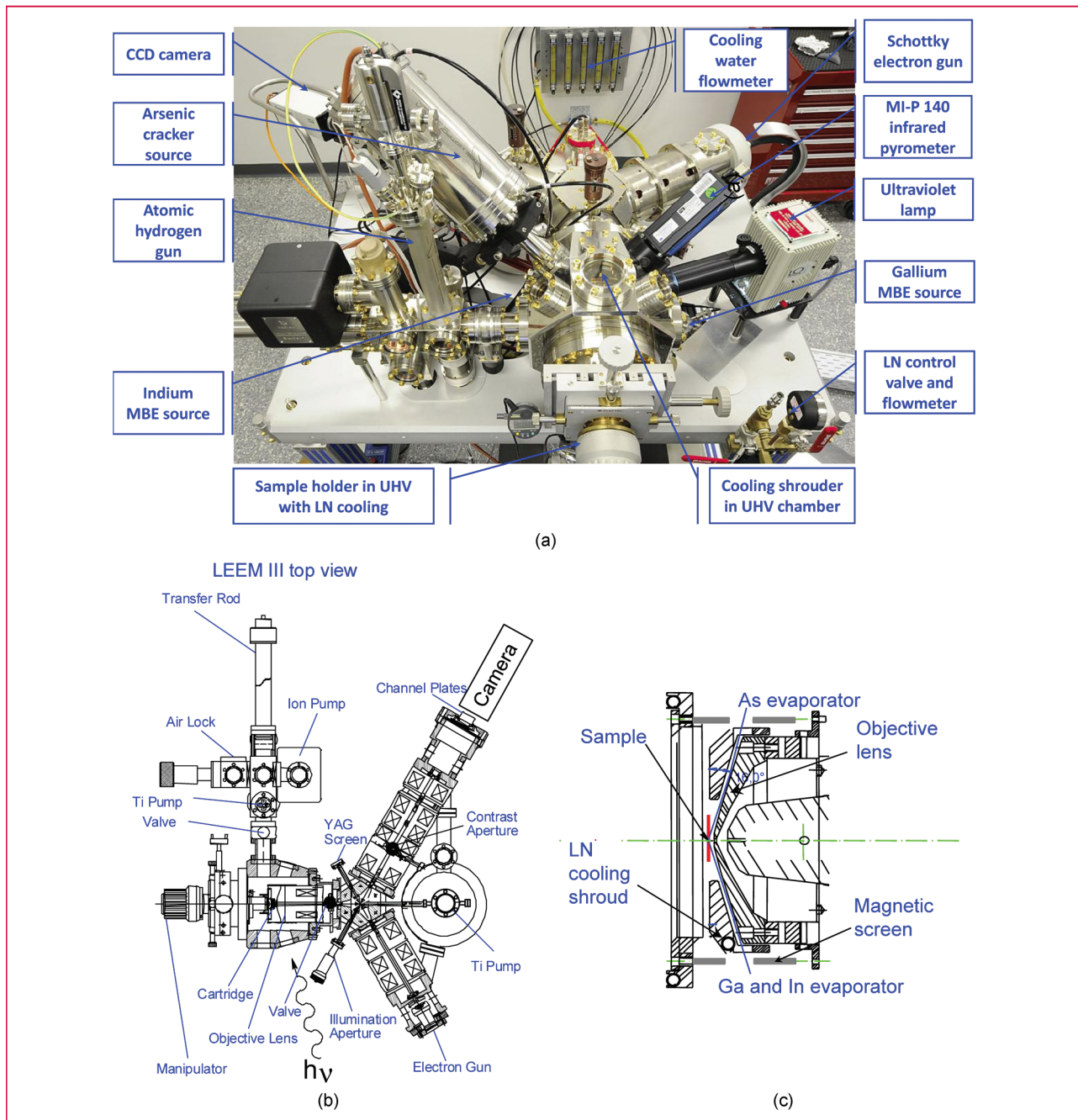


Figure 1
 (a) Image of the III-V LEEM system [7]. (b) Cross section of the III-V LEEM instrument. (c) Enlarged view of the objective lens area showing the location of the cooling shroud and access for the MBE sources. (CCD: charge-coupled device; YAG: yttrium–aluminum garnet.)

As cracker source (MBE-Komponenten). Since Ga and In are liquids at high temperature, it is necessary to mount the effusion cells in a face-up configuration [they are located underneath the instrument in Figure 1(a)]. Dual filaments are used to heat the crucibles to minimize droplet formation via

condensation near the orifice to improve flux reproducibility. Both sources are equipped with automatic shutters. In order to reduce material deposition in the objective lens region, a pyrolytic boron nitride cap with a small orifice, together with additional Ta shielding, ensures a well-collimated

evaporation beam. The Ga source is backed up by an uninterruptible power supply system to maintain the source temperature at 50°C and prevent cracking of the crucible in the event of a power failure.

The As cracker source consists of a 300-mL As reservoir, which is heated to evaporate the As. A cracking zone on top of the reservoir can be used to convert naturally sublimated As₄ into As₂ if required. An integrated all-metal valve between the reservoir and the cracking zone provides precise control of the As flux, which is important for dynamic imaging experiments. The reservoir and cracker temperature gradient is computer controlled during heating and cooling to reduce stress on the valve.

During III–V MBE, it is necessary to reduce the background As pressure resulting from high molecular As₄ or As₂ flux. Our III–V LEEM system therefore incorporates a cooling shroud for this purpose, which prevents discharge between the specimen and objective lens. The Cu shroud design is shown in Figure 1(c). Liquid nitrogen (LN) is supplied via a vacuum feedthrough to achieve thermal insulation. Small apertures in the shroud allow Ga, In, and As fluxes to impinge on the center of the sample. The background pressure is reduced by nearly 4 orders of magnitude when the shroud is in operation, which provides suitable conditions for imaging. However, following long time exposure to the As flux, the objective lens surface must be cleaned to reduce the probability of discharge. Magnetic shielding surrounds the cathode and anode regions in Figure 1(c) to screen the electron beam from stray fields originating from the MBE sources. An atomic hydrogen source (AHS) [8] is used for *in situ* surface cleaning of GaAs wafers. The AHS is effective at removing the surface oxide layer and surface impurities such as carbon. Several imaging modes such as LEEM and photoemission electron microscopy (PEEM) are applied in this paper [9–11].

Langmuir evaporation of GaAs

Langmuir (free) evaporation of GaAs(001) into a vacuum has been studied for many decades [12–15]. When heated, GaAs decomposes, and As and Ga fluxes evaporate from the surface. Below congruent evaporation temperature T_c , the fluxes are equal, preserving the compound stoichiometry. However, above T_c , As more readily evaporates, leaving behind Ga-rich droplets on the surface [16–19]. There has been a resurgence of interest in such droplets in the area of droplet epitaxy, where they are recrystallized under the As flux to generate GaAs quantum structures. Such structures can now be formed in different geometries, including dots, rings, and multirings with varied potential applications [20–22].

The formation and behavior of Ga droplets can be imaged by heating an epitaxy-ready (epi-ready) GaAs substrate above $T_c \sim 625^\circ\text{C}$ [15] in III–V LEEM. An undoped GaAs(001) $\pm 0.1^\circ$ epi-ready wafer was initially degassed at

300°C under ultrahigh vacuum for 24 hours in the LEEM system. This was followed by high-temperature flashing up to 600°C and annealing at 580°C for 2 hours to remove the surface oxide. Ga droplets were produced by annealing above T_c . The growth rate of the droplets is strongly dependent on annealing temperature, and this could be used to control their size. The base pressure of the system is below 2×10^{-10} torr, and typical pressures observed during imaging at the annealing temperature of 630°C are approximately 1×10^{-9} torr with LN cooling of the internal shroud.

Mirror electron microscopy (MEM), in which the specimen potential is adjusted so that electrons turn around just before the surface, is an ideal imaging mode for studying droplets [5, 6, 23–26]. A droplet distorts the uniform electric field between the planar sample surface and the objective anode, which significantly redistributes electron intensity. This can cause families of electron rays to overlap, creating strong caustic features in the image. For a large negative defocus range of the objective lens, droplets appear as dark circles enclosed by a bright caustic ring [see Figure 2(a)]. It should be noted that the caustic ring diameter in Figure 2(a) is larger than the actual perimeter of the droplet so that the droplet size is enlarged in MEM. This contrast can be understood and quantified from a numerical evaluation of classical electron ray trajectories [25].

Running Ga droplets

The most striking observation in III–V LEEM is that Ga droplets spontaneously “run” across the surface during annealing. Even after evaporation of many hundreds of monolayers of the crystal, the motion continues. Despite many studies of GaAs Langmuir evaporation over the years [12–17], to our knowledge, Ga droplet dynamics had not been previously observed, illustrating the advantages of *in situ* real-time imaging.

MEM images taken from movies of Ga droplet motion at three different temperatures are shown in Figure 2(a). The epi-ready surface is associated with slight roughness, and as the droplets move, they leave behind a smooth trail. The motion has a stick–slip character. It occurs preferentially along the [110] direction but equally in both directions, ruling out thermal gradient effects. It can be noted in Figure 2(a) that the size of the moving droplets decreases for $T < T_c$ and increases for $T > T_c$. At T_c , the droplet size remains stable, and surprisingly, there is a temperature range of approximately 20°C about T_c in which the droplets do not move. To further explore the relationship between motion and temperature, we adjusted the temperature to the desired T and measured the droplet velocity averaged over many minutes. The results are shown in Figure 2(b). Away from T_c , the average droplet velocity increases with either increasing or decreasing temperature. This unusual temperature dependence suggests that the motion is intimately linked to T_c .

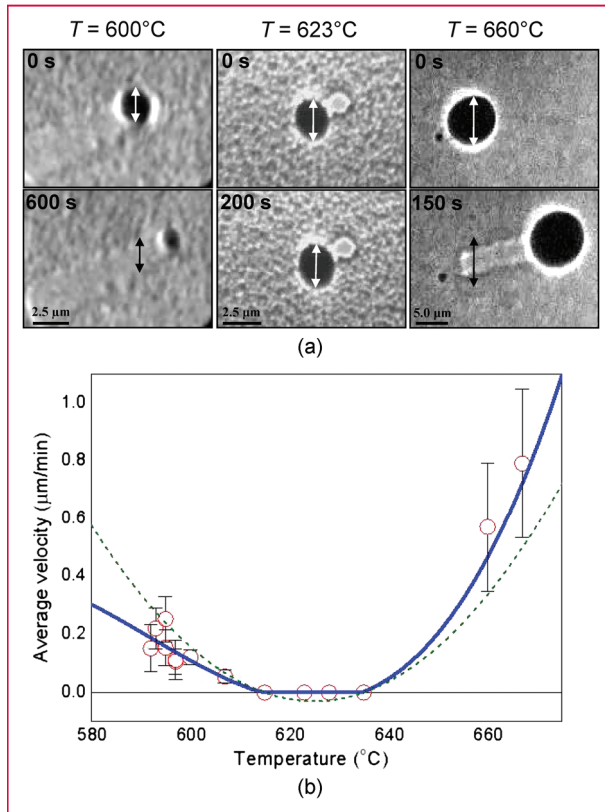


Figure 2

Droplet motion on epi-ready GaAs(001) [5]. (a) Image pairs are shown at successive times for three temperatures T as indicated; the center image pair is near the congruent evaporation temperature. Arrows are reference markers for comparing position and diameter at two times. The droplets (left panel) move and shrink below T_c and (right panel) move and grow above T_c . Close to T_c (center panel), there is no visible motion or size change. (b) Average velocity versus temperature. Error bars show root-mean-square scatter of multiple measurements at the same T . The solid line is the truncated cubic fit described in the text, and the dashed line is the quadratic term alone, which is extracted from the fit.

Guided by the experimental results, it would seem natural to consider the net force on the droplet derived from the thermodynamics of the GaAs surface during evaporation. The GaAs surface can be characterized by its surface Ga and As chemical potentials, i.e., μ_{Ga} and μ_{As} , respectively, where the sum $\mu_{\text{Ga}} + \mu_{\text{As}} = \mu_{\text{GaAs}}$ is fixed by equilibrium with the crystal, and μ_{GaAs} is the bulk crystal free energy per atom pair. Congruent evaporation at a given temperature T occurs because μ_{Ga} adjusts to a steady-state value where Ga and As evaporate at equal rates. Increasing T favors As evaporation, causing Ga to accumulate on the surface. Consequently, μ_{Ga} increases until the Ga and As evaporation rates are equal and congruent evaporation is restored. However, with increasing T , μ_{Ga} will eventually rise beyond

liquidus value μ_L , and Ga can nucleate as liquid droplets rather than all evaporating. This defines the upper limit T_c for congruent evaporation. It is expected that the Ga droplets will stay close to equilibrium with the GaAs crystal at μ_L , which gives rise to a disequilibrium between the droplet and the surface for temperatures away from T_c , where $\mu_{\text{Ga}} \neq \mu_L$.

To see how the disequilibrium in chemical potential results in motion, it is necessary to consider the net force on a droplet when it is displaced (e.g., by a thermal fluctuation). Integrating the force vector around the periphery of the droplet, it can be shown that the total net force on a droplet is proportional to the difference in Gibbs free surface energy of the surfaces exposed and covered during the motion [5]. The newly exposed surface is created in equilibrium with the droplet at chemical potential μ_L . However, before being covered by the droplet, the surface on the opposite side had a structure corresponding to μ_{Ga} , whereas the reservoir for the excess Ga is now the droplet at μ_L . Expanding to the lowest order in $(T - T_c)$, one finds that the difference in free surface energy is quadratic in $(\mu_{\text{Ga}} - \mu_L)$ and that $(\mu_{\text{Ga}} - \mu_L)$ is linear in $(T - T_c)$, giving the total net force on a droplet of diameter d at temperature T as

$$F = \alpha(T - T_c)^2 d, \quad (1)$$

where coefficient α embodies both thermodynamic and kinetic properties of the surface [5]. Modeling the time-averaged stick-slip motion as a damped response to F with an effective frictional force that is independent of velocity and opposite to the direction of motion, then from Equation (1), the velocity becomes

$$v \approx m\alpha(T - T_c)^2 - \nu_f, \quad (2)$$

where m is the mobility, and ν_f is the friction term. For $(T - T_c)^2 < \nu_f/m\alpha$, $v = 0$, which is consistent with the region of zero motion about T_c . When the range of T is large, it is necessary to include cubic and higher order terms in the expansion about T_c , and with Equation (2) extended to cubic order, it is possible to fit (solid blue line) the velocity data well, as shown in Figure 2(b). The basic prediction of $v \propto (T - T_c)^2$ is, however, sufficient to capture the overall general behavior.

We note that there have been a number of interesting studies of droplet dynamics on surfaces with different proposed mechanisms for motion [27–29]. The mechanism for running droplets described here should be applicable to other III–V semiconductors such as InAs, where the more slowly evaporating component forms droplets on the surface at temperatures where a liquidus exists. More broadly, the droplet motion may create new possibilities to position nanostructures in droplet epitaxy.

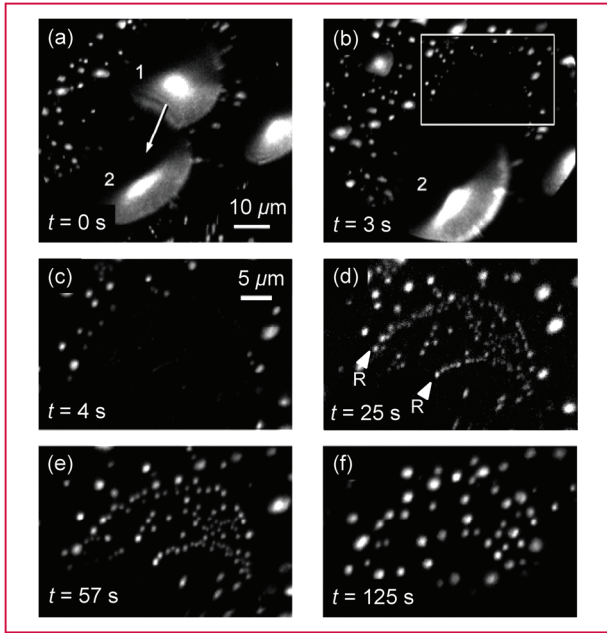


Figure 3

Images captured from a PEEM video of Ga droplet coalescence at 630°C [6]. Liquid Ga appears bright against dark GaAs. (a) Droplets 1 and 2 are in close proximity at $t = 0$. (b) At $t = 3$ seconds, droplet 1 translates across the substrate and coalesces with droplet 2, leaving an exposed shallow etch pit. This exposed etch pit, which is enclosed by the frame in (b), is magnified in (c)–(f). (c) Daughter droplet formation and (d) growth are sometimes associated with surface ridges, R.

Droplet coalescence during Langmuir evaporation

Above T_c , excess Ga is left behind during evaporation and diffuses to the droplets, which grow via adatom capture. Occasionally, however, droplets also abruptly grow via coalescence [6, 9]. These events are particularly interesting, as illustrated by the sequence of PEEM images shown in **Figure 3**. Droplet 1 in Figure 3(a) is absorbed into droplet 2 (which remains stationary) in a coalescence event [see Figure 3(b)]. This leaves behind the etch pit framed in Figure 3(b) and magnified in Figure 3(c). Within 2 seconds, a rapid burst of daughter droplet nucleation occurs within this area. Following rapid growth, they begin to move at $t = 51$ seconds. Eventually, the droplets move outside the etch pit arena, and there is no subsequent nucleation suggesting an unanticipated nucleation mechanism.

To elucidate the mechanism, we employ MEM [5, 6, 23–26] to reveal information on surface morphology. In particular, MEM movies of coalescence events similar to Figure 3 reveal that the concave etch pit left behind by the coalescing droplet planarizes with time, and only then do the daughter droplets move away from the region. The time for significant planarization corresponds to the initial burst of

nucleation and growth of the daughter droplets with no further nucleation occurring after the surface is planarized.

Simple model for Langmuir evaporation of GaAs

The linkage between planarization and droplet formation suggests that surface steps are important, and we develop a simple model of Langmuir evaporation from a miscut wafer of mean step spacing L_s . Our assumption is that Ga adatoms persist on the surface long enough to maintain approximate equilibrium between terrace and steps [30]. However, it is known that As readily evaporates, and a constant excess flux of As is required to prevent decomposition during MBE [15]. Consequently, we assume that, at our experimental temperatures, As surface species evaporate too rapidly to maintain a significant population across the terrace. Then, the rate of As evaporation is proportional to step density, whereas Ga evaporation is independent of step density. Formalizing this using a standard transition-state model for As and Ga evaporation, the evaporation rates per unit area are

$$F_{\text{Ga}} = r_{\text{Ga}} \exp\left(\frac{\mu_{\text{Ga}} - E_{\text{Ga}}}{kT}\right) \quad (3)$$

$$F_{\text{As}} = r_{\text{As},s} L_s^{-1} \exp\left(\frac{N(\mu_{\text{GaAs}} - \mu_{\text{Ga}}) - E_{\text{As}N}}{kT}\right). \quad (4)$$

Here, E_{Ga} and $E_{\text{As}N}$ are the respective transition-state energy values for Ga and As evaporation, and it is assumed that the As transition state consists of N atoms. The rate constants r_{Ga} (per unit area) and $r_{\text{As},s}$ (per unit step length) include the transition-state entropy or degeneracy, for example, the density of sites for evaporation. As discussed earlier, μ_{Ga} increases with increasing T until $F_{\text{Ga}} = F_{\text{As}}$. However, if μ_{Ga} rises above the liquidus value, Ga can accumulate as droplets, which defines T_c . Inserting Equations (3) and (4) in the condition $F_{\text{Ga}} = F_{\text{As}}$ for $\mu_{\text{Ga}} = \mu_L$ then yields an expression for the congruent evaporation temperature, i.e.,

$$kT_c = \frac{(N+1)\mu_L - N\mu_{\text{GaAs}} - E_{\text{Ga}} + E_{\text{As}N}}{\ln(r_{\text{As},s}/L_s r_{\text{Ga}})}. \quad (5)$$

This simple model leads to several important predictions [6]. First, above T_c , if droplet coalescence suddenly exposes an etch pit of much higher local miscut, then that region will experience much faster As evaporation and Ga release, explaining the burst of nucleation and subsequent growth of the daughter droplets. Second, the release of Ga increases μ_{Ga} in the etch pit region. This drives the surface further from the liquidus composition, which enhances the force for the droplet motion [5] and accounts for the rapid daughter droplet dynamics. Finally, it can be observed in Equation (5) that T_c depends on the miscut via mean step spacing L_s . This has potential implications for positioning nanostructures, which we consider in the next section.

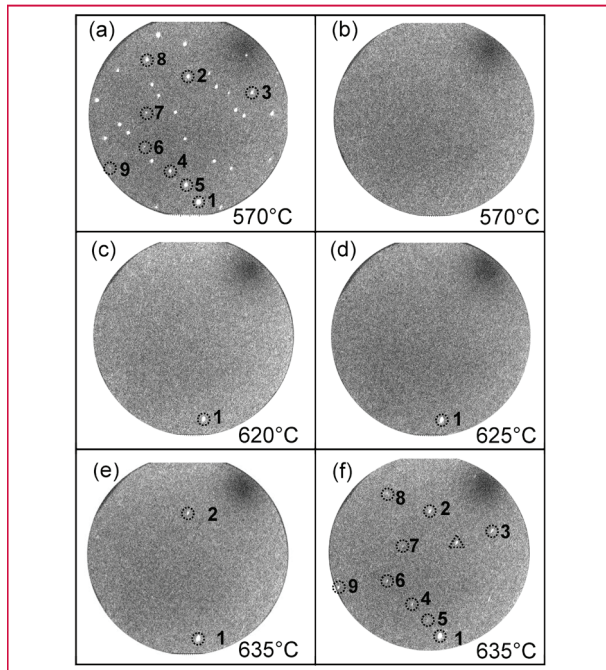


Figure 4

PEEM images of Ga droplet shrinkage and formation [6]. (a) The sample is cooled below T_c so that Ga droplets shrink and eventually disappear in (b). Circled droplet 1 in (a) is the largest droplet and the last to disappear. (c) On slowly heating the sample to 620°C, a new droplet is generated in the original position of droplet 1. (d) This droplet was stable in the temperature range of 620°C–625°C for several minutes. (e) Increasing the temperature to 635°C results in an additional droplet appearing at the original position of droplet 2 in (a). (f) After a further minute at 635°C, 90% of the new droplets correspond to previous droplet positions in (a) (circled droplets). The droplet enclosed by a triangle has appeared at a new position.

Positioning nanostructures using spatial variations in T_c

Equation (5) indicates that the regions of the surface possessing a higher local miscut will have a lower T_c , suggesting new possibilities for controlled nanostructure formation on lithographically patterned substrates. Evaporation should preferentially occur on the most highly sloped regions, allowing generation of droplets at predetermined locations. Annealing at temperatures above T_c for the sloped regions, but below T_c for the surrounding planar surface, should provide especially reliable Ga placement. The droplets could then be converted into quantum structures under an overpressure of a group V vapor as in standard droplet epitaxy methods [2, 20–22].

We have demonstrated droplet positioning at a proof-of-concept level. We first heated a GaAs(001) sample above T_c to form a number of well-separated Ga droplets [see **Figure 4(a)**]. The sample was then cooled below T_c

so that the Ga droplets shrink and eventually disappear [see **Figure 4(b)**]. This leaves a surface patterned with nanoscale depressions due to droplet etching. The largest droplet, which is designated 1 in **Figure 4(a)**, is associated with the deepest etch pit and was the last to disappear. When we slowly increase the temperature to 620°C, a new droplet appears at precisely the same position as that of droplet 1 [see **Figure 4(c)**]. We can control the stability of this single droplet over a significant time period (many minutes) and temperature range $\pm 5^\circ\text{C}$ [see **Figure 4(d)**]. On increasing the temperature to 635°C, a new droplet is generated in the etch pit previously occupied by droplet 2 [see **Figure 4(e)**]. Even after 1 minute of annealing at 635°C, approximately 90% of the new droplets generated in **Figure 4(f)** correspond to etch pit positions. This demonstrates that droplet positions can be controlled by surface patterning.

Conclusion

We have described the design of a III–V surface electron microscope and its application to study Langmuir evaporation of GaAs(001). Droplets move during evaporation, which is driven by disequilibrium with the surface, giving rise to an unusual temperature dependence. Coalescence events are associated with the nucleation and motion of numerous “daughter droplets.” These observations indicate a morphology-dependent congruent evaporation temperature, which has important implications for writing nanostructures.

Acknowledgments

The work of D. E. Jesson and W.-X. Tang was supported by the Australian Research Council under grant DP0985290. We thank Rod Mackie for technical support.

References

1. B. A. Joyce and D. D. Vvedensky, “Self-organized growth on GaAs surfaces,” *Mater. Sci. Eng. R*, vol. 46, no. 6, pp. 127–176, Dec. 2004.
2. J. H. Lee, Z. M. Wan, Z. Y. AbuWaar, and G. J. Salamo, “Design of nanostructure complexes by droplet epitaxy,” *Cryst. Growth Des.*, vol. 9, no. 2, pp. 715–721, Jan. 2009.
3. S. Kiravittaya, A. Rastelli, and O. G. Schmidt, “Advanced quantum dot configurations,” *Rep. Prog. Phys.*, vol. 72, no. 4, article no. 046502, Mar. 2009.
4. D. Spirkoska, C. Colombo, M. Heiss, G. Abstreiter, and A. F. I. Morral, “The use of molecular beam epitaxy for the synthesis of high purity III–V nanowires,” *J. Phys. Condens. Matter*, vol. 20, no. 45, article no. 454225, Nov. 2008.
5. J. Tersoff, D. E. Jesson, and W. X. Tang, “Running droplets of Ga from evaporation of Ga arsenide,” *Science*, vol. 324, no. 5924, pp. 236–238, Apr. 2009.
6. J. Tersoff, D. E. Jesson, and W. X. Tang, “Decomposition controlled by surface morphology during Langmuir evaporation of GaAs,” *Phys. Rev. Lett.*, vol. 105, no. 3, p. 035702, Jul. 2010.
7. D. E. Jesson and W. X. Tang, “Surface electron microscopy of Ga droplet dynamics on GaAs (001),” in *Microscopy: Science, Technology, Applications and Education*, A. Méndez-Vilas and J. Díaz, Eds. Badajoz, Spain: Formatex, 2010, pp. 1608–1619.

8. K. G. Tschersich and V. von Bonin, "Formation of an atomic hydrogen beam by a hot capillary," *J. Appl. Phys.*, vol. 84, no. 8, pp. 4065–4070, Oct. 1998.
9. E. Bauer, "Low energy electron microscopy," *Rep. Prog. Phys.*, vol. 57, no. 9, pp. 895–938, Sep. 1994.
10. A. B. Pang, T. Müller, M. S. Altman, and E. Bauer, "Fourier optics of image formation in LEEM," *J. Phys. Condens. Matter*, vol. 21, no. 31, article no. 314006, Jul. 2009.
11. S. Günther, B. Kaulich, L. Gregoratti, and M. Kiskinova, "Photoelectron microscopy and applications in surface and materials science," *Prog. Surf. Sci.*, vol. 70, no. 4–8, pp. 187–260, Jul. 2002.
12. C. T. Foxon, J. A. Harvey, and B. A. Joyce, "The evaporation of GaAs under equilibrium and non-equilibrium conditions using a modulated beam technique," *J. Phys. Chem. Solids*, vol. 34, no. 10, pp. 1693–1701, Oct. 1973.
13. J. R. Arthur, "Vapor pressures and phase equilibria in the Ga–As system," *J. Phys. Chem. Solids*, vol. 28, no. 11, pp. 2257–2267, Nov. 1967.
14. B. Goldstein, D. J. Zostak, and V. S. Ban, "Langmuir evaporation from the (100), (111A), and (111B) faces of GaAs," *Surf. Sci.*, vol. 57, no. 2, pp. 733–740, Jul. 1976.
15. J. Y. Tsao, *Materials Fundamentals of Molecular Beam Epitaxy*. 1st ed. San Diego, CA: Academic, 1993.
16. M. Zinke-Allmang, L. C. Feldman, and W. van Saarloos, "Experimental study of self-similarity in the coalescence growth regime," *Phys. Rev. Lett.*, vol. 68, no. 15, pp. 2358–2361, Apr. 1992.
17. T. D. Lowes and M. Zinke-Allmang, "Microscopic study of cluster formation in the Ga on GaAs(001) system," *J. Appl. Phys.*, vol. 73, no. 10, pp. 4937–4941, May 1993.
18. Z. Y. Zhou, C. X. Zheng, W. X. Tang, D. E. Jesson, and J. Tersoff, "Congruent evaporation temperature of GaAs(001) controlled by As flux," *Appl. Phys. Lett.*, vol. 97, no. 12, article no. 121912, Sep. 2010.
19. Z. Y. Zhou, W. X. Tang, D. E. Jesson, and J. Tersoff, "Time-evolution of the Ga droplet size-distribution during Langmuir evaporation of GaAs (001)," *Appl. Phys. Lett.*, vol. 97, no. 19, article no. 191914, Nov. 2010.
20. T. Mano, T. Kuroda, S. Sanguinetti, T. Ochiai, T. Tateno, J. Kim, T. Noda, M. Kawabe, K. Sakoda, G. Kido, and N. Koguchi, "Self-assembly of concentric quantum double rings," *Nano Lett.*, vol. 5, no. 3, pp. 425–428, Mar. 2005.
21. M. Yamagiwa, T. Mano, T. Kuroda, T. Tateno, K. Sakoda, G. Kido, N. Koguchi, and F. Minami, "Self-assembly of laterally aligned quantum dot pairs," *Appl. Phys. Lett.*, vol. 89, no. 11, article no. 113115, Sep. 2006.
22. C. Somaschini, S. Bieti, N. Koguchi, and S. Sanguinetti, "Fabrication of multiple concentric nanoring structures," *Nano Lett.*, vol. 9, no. 10, pp. 3419–3424, Sep. 2009.
23. S. M. Kennedy, C. X. Zheng, W. X. Tang, D. M. Paganin, and D. E. Jesson, "Laplacian image contrast in mirror electron microscopy (addendum)," *Proc. R. Soc. A.*, May 18, 2011, published online, DOI: 10.1098/rspa.2011.9204.
24. S. M. Kennedy, C. X. Zheng, W. X. Tang, D. M. Paganin, and D. E. Jesson, "Laplacian image contrast in mirror electron microscopy," *Proc. Roy. Soc. A*, vol. 466, no. 2122, pp. 2857–2874, Oct. 2010.
25. S. M. Kennedy, C. X. Zheng, W. X. Tang, D. M. Paganin, and D. E. Jesson, "Caustic imaging of gallium droplets using mirror electron microscopy," *Ultramicroscopy*, vol. 111, no. 5, pp. 356–363, Apr. 2011.
26. S. M. Kennedy, D. E. Jesson, and D. M. Paganin, "Laplacian and caustic imaging theories of MEM work-function contrast," *IBM J. Res. Dev.*, vol. 55, no. 4, paper 3, pp. 3:1–3:8, 2011.
27. E. Hilner, A. A. Zakharov, K. Schulte, P. Kratzer, J. N. Andersen, E. Lundgren, and A. Mikkelsen, "Ordering of the nanoscale step morphology as a mechanism for droplet self-propulsion," *Nano Lett.*, vol. 9, no. 7, pp. 2710–2714, Jun. 2009.
28. W. C. Yang, H. Ade, and R. J. Nemanich, "Stability and dynamics of Pt–Si liquid microdroplets on Si(001)," *Phys. Rev. B, Condens. Matter*, vol. 69, no. 4, article no. 045421, Jan. 2004.
29. P. Sutter, P. A. Bennett, J. I. Flege, and E. Sutter, "Steering liquid Pt–Si nanodroplets on Si(100) by interactions with surface steps," *Phys. Rev. Lett.*, vol. 99, no. 12, article no. 125504, Sep. 2007.
30. J. Tersoff, M. D. Johnson, and B. G. Orr, "Adatom densities on GaAs: Evidence for near-equilibrium growth," *Phys. Rev. Lett.*, vol. 78, no. 2, pp. 282–285, Jan. 1997.

Received September 28, 2010; accepted for publication January 19, 2011

Wen-Xin Tang *School of Physics, Monash University, Victoria, 3800, Australia* (wenxin.tang@monash.edu). Dr. Tang received his B.S. degree from Xinjiang University and his Ph.D. degree from Fudan University in China. He subsequently joined the Max Planck Institute of Microstructure Physics in Germany, where his research has involved studying surface magnetism. He is a Research Fellow in the School of Physics at Monash University. Currently, he is focused on the development of III–V low-energy electron microscopy.

Chang-Xi Zheng *School of Physics, Monash University, Victoria, 3800, Australia* (changxi.zheng@monash.edu). Mr. Zheng is a Ph.D. student in the School of Physics at Monash University in Australia. He received a B.S. degree in materials physics from Lanzhou University in 2004, and he obtained his M.Sc. degree in material physics and engineering from Sun Yat-sen University in 2007 in China. In 2008, he commenced his Ph.D. research on GaAs(001) surface dynamics studied by low-energy electron microscopy.

Zhen-Yu Zhou *School of Physics, Monash University, Victoria, 3800, Australia* (zhenyu.zhou@monash.edu). Mr. Zhou is a Ph.D. student in the School of Physics at Monash University. He received his B.S. degree from Peking University in China, and he received a Master's degree in material physics and chemistry in the Institute of Semiconductors, Chinese Academy of Sciences. Since 2008, his Ph.D. project has focused on the study of nanoscale surface dynamics of III–V semiconductors using low-energy electron microscopy.

David E. Jesson *School of Physics, Monash University, Victoria, 3800, Australia* (david.jesson@monash.edu). Professor Jesson received his B.Sc. and Ph.D. degrees in physics from Bristol University in the United Kingdom. He has previously held positions at the CSIR (Council for Scientific and Industrial Research, South Africa), Oak Ridge National Laboratory, and Heriot-Watt University in Edinburgh. He joined Monash in 2003. His work involves the use of novel electron microscopy techniques to study semiconductor growth mechanisms. Most recently, he has pioneered the development and application of a III–V surface electron microscope.

Jerry Tersoff *IBM Research Division, Thomas J. Watson Research Center, Yorktown Heights, New York 10598 USA* (tersoff@us.ibm.com). Dr. Tersoff is a Research Staff Member at the IBM Thomas J. Watson Research Center. He received a B.A. degree in physics from Swarthmore College, and a Ph.D. degree in physics from the University of California, Berkeley. His work spans diverse topics in the theoretical understanding of surfaces, interfaces, electronic materials, epitaxial growth, and nanoscale devices.